Article

Plasmonic nanosensor array for multiplexed DNA-based pathogen detection

David Zopf, Angelina Pittner, André Dathe, Norman Grosse, Andrea Csáki, Kai Arstila, J. Jussi Toppari, Walter Schott, Denis Dontsov, Günter Uhlrich, Wolfgang Fritzsche, and Ondrej Stranik

ACS Sens., **Just Accepted Manuscript** • DOI: 10.1021/acssensors.8b01073 • Publication Date (Web): 18 Jan 2019

Plasmonic nanosensor array for multiplexed DNA-based pathogen detection

*David Zopf[1], Angelina Pittner[1], André Dathe[1,2], Norman Grosse[1], Andrea Csáki[1], Kai Arstila[3], J. Jussi Toppari[3], Walter Schott[4], Denis Dontsov[4], Günter Uhlrich[5], Wolfgang Fritzsche[1] and Ondrej Stranik[1]**

[1]Leibniz Institute of Photonic Technology (IPHT) Jena, Member of the Leibniz Research Alliance - Leibniz Health Technologies, Albert-Einstein-Straße 9, 07745 Jena, Germany

[2]Jena University Hospital, Friedrich-Schiller-University, Teichgraben 8, 07743 Jena, Germany

[3]University of Jyväskylä, Department of Physics and Nanoscience Center, P.O. Box 35, 40014 University of Jyväskylä, Finland

[4] SIOS Meßtechnik GmbH, Am Vogelherd 46, 98693 Ilmenau, Germany

[5]ABS Gesellschaft für Automatisierung, Bildverarbeitung und Software mbH, Stockholmer Straße 3, 07747 Jena, Germany

*corresponding author: ondrej.stranik@leibniz-ipht.de

Abstract

In this research we introduce a plasmonic nanoparticle based optical biosensor for monitoring of molecular binding events. The sensor utilizes spotted gold nanoparticle arrays as sensing platform. The nanoparticle spots are functionalized with capture DNA sequences complementary to the analyte (target) DNA. Upon incubation with the target sequence, it will bind on the respectively complementary functionalized particle spot. This binding changes the local refractive index, which is detected spectroscopically as the resulting changes of the localized surface plasmon resonance (LSPR) peak wavelength. In order to increase the signal, a small gold nanoparticle label is introduced. The binding can be reversed using chemical means (10 mM HCl). It is demonstrated that a multiplexed detection and identification of several fungal pathogen DNA sequences subsequently on one sensor array is possible by this approach.

Keywords: LSPR sensing, plasmonic nanoparticles, DNA detection, plasmonic array, Fourier-transform-imaging spectroscopy

A fast and cost-efficient identification of a variety of pathogens in different matrices (air, water, food, blood, etc.) represents a major challenge in today's bioanalytics and medical diagnostics. Although immunosensing is widely established [1] and routinely used, it is increasingly complemented by nucleic acid-based detection approaches due to the capability to identify species and strains of pathogens [2]. Pathogens are usually identified based on their specific DNA, which is detected by highly selective binding (hybridization) to single-stranded DNA molecules of complementary base sequence. This recognition reaction can result in an amplification (such as PCR), or the enrichment of target DNA on a sensor surface, which can be read out optically based on color staining or fluorescent labels, electrochemically by changes in mass (QCM) [3,4] or refractive index (SPR, LSPR) [5,6], by magnetic labels [7], etc.

For single detection reaction both simple (lateral flow) [8] as well as more sophisticated (real-time PCR) approaches are established and utilized [9,10]. However, if a larger number of assays are required for one

sample, these methods scale poorly and are limited due to sample volume, reproducibility as well as price issues. Thus, multiplexed approaches, which provide a larger potential for integration of assays, preferably in a miniaturized format, are desperately needed. In the case of nucleic acid -based assays, a solution to this problem could be the combination of a multiplexed and/or consensus DNA-amplification (such as PCR), that amplifies all target DNA of interest and results in a mixture of amplification (PCR) products [11,12]. Subsequently, identification of the various possible mixture components is realized by a microarray hybridization step, where complementary (capture) DNA molecules are attached in an array of spots on a solid substrate surface. Again, any bound ensemble of target DNA has to be detected on the surface, which is usually done by fluorescence readout of labels on the target molecules [13,14].

Although optical readout is clearly preferred in multiplex arrangements, fluorescence detection exhibits serious limitations. The use of labels might alter the intrinsic properties. Also additional steps, and therefore higher time and cost requirements are required, as well as an inherently limited signal stability (photobleaching) [15,16]. Another optical readout approach is based on surface plasmon resonance (SPR), an effect observed at the interface between a metal surface and a dielectric, based on interaction of light with the conduction electrons in the metal. This resonance is influenced by binding of the target molecules on the metal surface. The change in resonance can be detected based on a change of the angular or wavelength spectrum of incident light coupled to the surface plasmon [17]. The incoupling of light requires a prism, grating or wave guide arrangement, thereby seriously limiting integration and miniaturization abilities [18]. An interesting alternative based on a similar effect of light interaction with conduction electrons in metals, but in much smaller, nanoscale structures, is represented by localized surface plasmon resonance (LSPR) [19]. Here, metal nanostructures interact directly with light, requiring no dedicated technical arrangement, and allowing for extreme miniaturization [20]. The binding of the target DNA from solution to the complementary capture DNA (attached to the surface of metal nanostructures) results in a change (red-shift because increase in effective refractive index) of the resonance peak wavelength of this nanoparticle, which is measured and forms the sensor signal. Using this approach, the sequence-specific detection of DNA using a single 80 nm gold nanoparticle as a sensor was demonstrated [21].

In the fluorescence microscopy detection scheme, a regular array of spots, each one functionalized with a specific capture DNA, is fabricated. The presence of the target DNA is manifested as a bright spot at specific position, because the complementary DNA is fluorescently-labeled. This concept can be transferred to the LSPR field by fabrication of an array of spots involving metal structures and functionalized with a specific capture DNA sequence. Although the proof-of-principle of LSPR DNA sensors could be demonstrated, the full multiplexing potential was not yet realized. Ruemmele et al. demonstrated a parallel spectroscopic read-out of isolated circular regions of nanodisk arrays modified by hand with a pipette [22].

Theoretically, each single particle with different capture molecules could act as an independent sensor. However, this demands independent and well controlled conjugation of each nanoparticle with different capture DNA. So far, such multiplexed conjugation was demonstrated by the technique of a time-sequential adsorption of nanoparticles and bio-conjugation [23,24]. However, this approach is hardly practical. It requires a single particle resolution, and does not allow routine applications outside of the research laboratory. Therefore, micro spots of metal nanoparticles were used, because they can be easily independently modified by capture DNAs. To fabricate the metal nanoparticles, two general approaches

are possible, lithographic (top-down) or self-assembly (bottom-up). Although lithographic approaches allow for a high-precision of the geometry of each sensor, and also the arrangement of the spots, it has the drawback of higher costs based on the required clean-room technologies. The last decades have witnessed the development of simpler replication tools such as soft-lithography including nanoimprint, improving the access to such technologies [25,26]. On the other hand, the bottom-up side could be realized using chemically synthesized metal nanoparticles, which have superior plasmonic properties due to their crystallinity, compared to the rather polycrystalline lithographic sensors [27].

Here we present the utilization of chemically synthesized nanostructures, using immobilization technologies - for both particles as well as for the attachment of capture DNA molecules – which are established in the DNA microarray field. The schematics of this new approach are in Figure 1.

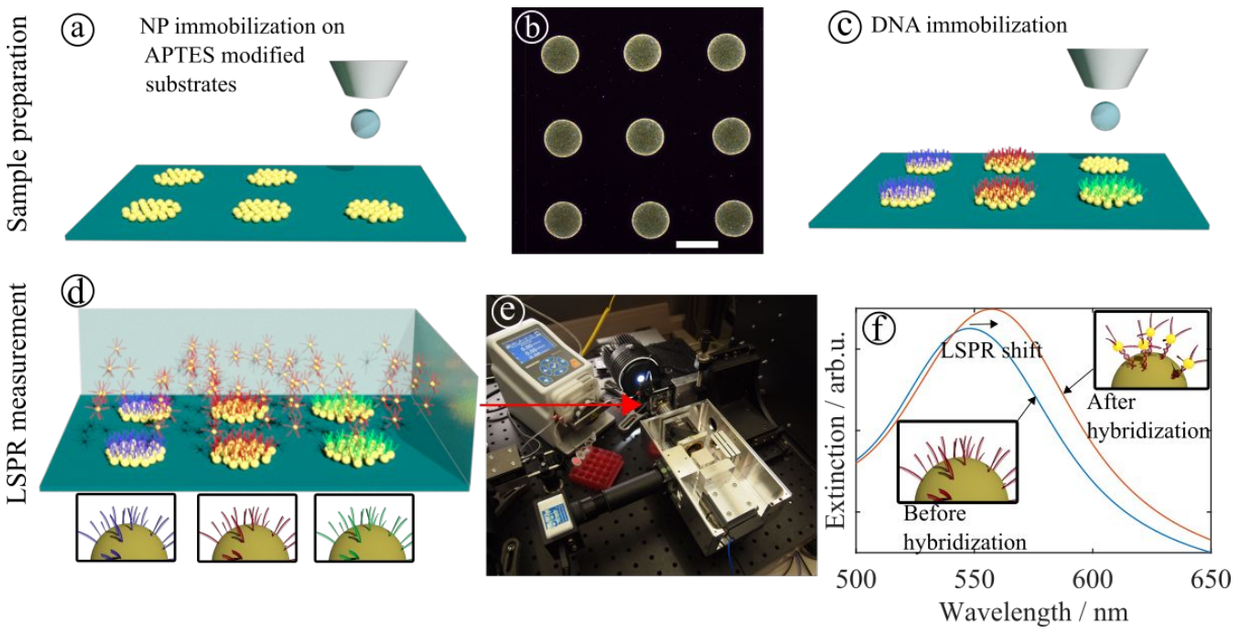

Figure 1. Schematic of the sample preparation and measurement principle. (a) Nanoparticle immobilization on APTES modified glass substrates by a piezoelectric dispenser system. (b) Dark-field image of the resulting nanoparticle spot array (scale bar = 200 µm). (c) After a washing step and ozone cleaning the nanoparticle spots were functionalized (by spotting) with various thiolated DNA sequences. (d) Subsequently the plasmonic microarray was integrated in a microfluidic chamber and the measurement of the whole assay was conducted by a Fourier-transform imaging spectrometer shown in (e). (f) Sensing priciple of the LSPR microarray. Upon the introduction of labeled complementary DNA sequences in the chamber, it will bind to capture DNA (which is immobilized on certain particle spots), thereby change the local refractive indes, which can be measured as a peak shift by the imaging spectrometer.

We used chemically synthesized gold nanoparticles (diameter 80 nm) as sub-monolayer in a spot array on a glass substrate where each spot is subsequently modified separately with a specific capture DNA sequence. Binding of the capture strands was enabled by the reaction of a terminal thiol functional group with the gold particle surface. Thus, when located in a flow chamber and incubated with a solution containing target DNA, this DNA will bind specifically to the spot with the complementary capture DNA. This binding induces a change of the spectroscopic properties of this spot (red-shift of the LSPR peak position), which is monitored by a Fourier-transform imaging spectrometer. The sensitivity of the assay is enhanced by conjugation of DNA with small nanoparticles (this step requires pre-treatment of the sample by DNA amplification technique (PCR)). The multiplexing ability of this setup is successfully demonstrated for the detection of various pathogenic fungi and their identification. Control experiments using other DNA sequences demonstrated the high specificity of the hybridization-based approach.

Results and Discussion

To obtain the extinction spectra of a single nanoparticle spot, the hyperspectral data cube is cropped by object recognition into regions of interest (ROIs), each including one nanoparticle spot in the center of the cropped hyperspectral cube (see red outline in Figure 2a). Figure 2a shows the intensity of the spot array including 50 nanoparticle spots at 519.8 nm. The nanoparticle spots appear as dark greyish regions while the background appears brighter. The background intensity $I_0(x,y,\lambda)$ under the nanoparticle spot is interpolated by a hyperbolic surface fit. The nanoparticle spot and disturbances in the background are excluded in the calculation of the surface fit. Subsequently, the hyperspectral image slice is normalized on the background (see Figure 2c). The interpolation of the background and normalization is performed for all wavelength slices of the hyperspectral data cube. Chromatic aberration leads to lateral shifts in the x and y position between the wavelength slices of the hyperspectral data cube. These shifts are calculated by cross-correlating the normalized image slice $N(x,y,\lambda)$ of the smallest wavelength with all consecutive wavelength slices. The obtained shift vectors are then used to correct for the shifts between the wavelengths slices. Locations of nanoparticles are identified by object recognition (green outline in Figure 2d). Due to the manufacturing process the distribution of the nanoparticles in the spots is not completely homogenous. Especially close to the edges the nanoparticle density is higher (see dark field image in Figure 1b). Furthermore there might be disturbances in the distribution due to dust particles, or areas where no nanoparticles attach. These areas are identified and excluded. The LSPR positions of the extinction spectra were determined if not stated otherwise as in Dahlin et al. [28].

The typical arrangement of the nanoparticles spot array is visible in the optical overview in Figure 2a: Spots of about 200 µm in diameter are fabricated in a 5x10 arrangement on a chip. In order to obtain the spectroscopic properties of each individual spot, the following image processing routines are utilized: Object recognition based on thresholding extracts the individual spots from the background (Figure 2b), and the background intensity is extrapolated for each wavelength slice (Figure 2c). Then, an averaged extinction spectrum is calculated of the given spot (Figure 2d). The high reproducibility of the measurements including the subsequent image processing routine is demonstrated in Figure 2d for 10 different measurements of the very same spot. This achieved reproducibility ensures that the spectral shifts can be reliably detected.

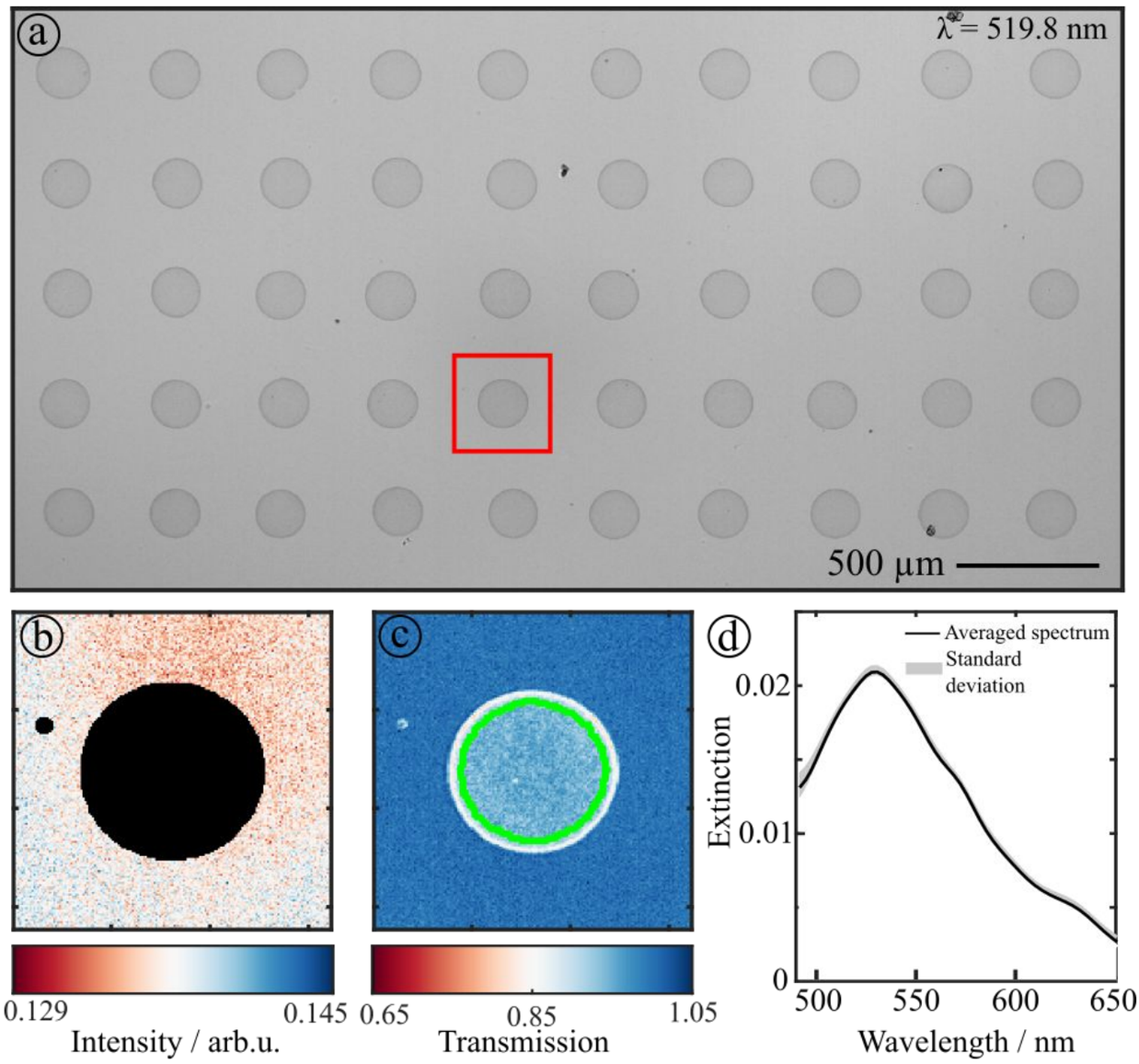

Figure 2. Image processing steps to calculate the extinction spectrum of a single nanoparticle spot. (a) Calculated bright field image of a nanoparticle spot array on glass at 519.8 nm. (b) Input area $\boldsymbol{I_0(x,y,\lambda = 519.8\,nm)}$ for the calculation of the hyperbolic surface fit used to extrapolate the background intensity under the nanoparticle spot. (c) Hyperspectral image slice after normalization by the calculated surface fit. (d) Averaged extinction spectrum of 10 subsequent measurements of the tagged nanoparticle spot. The standard deviation is plotted as grey area.

Characterization of spots

Ten measurements on 50 not-yet functionalized particle spots in air were conducted to check for possible variations introduced by the manufacturing process of the spots. The LSPR extinction spectrum of each spot was obtained using the procedure described above (see Figure 2) and the LSPR peak position was determined by calculating the peak maximum of the extinction spectrum of each nanoparticle spot. Figure 3a shows the extinction spectra averaged over 10 measurements of all spots. Figure 4b shows the distribution of the peak maxima of these nanoparticle spots. The LSPR peak maxima range from 527.4 nm to 530.7 nm with an average of $\mu = 529.3$ nm ($\sigma = 0.7\ nm$). The analysis showed that the generation of sensor spots using a piezoelectric dispenser system leads to remarkably reproducible extinction spectra of the fabricated spots. As a measure of the instrument's uncertainty of peak determination the standard deviation of the LSPR peak maxima obtained from ten measurements was calculated for each sensor spot. The distribution is shown in the inset in Figure 4b. The average standard deviation was 0.9 nm.

To estimate the particle density in the center region of a nanoparticle spot, an AFM measurement of a surface area of 100 µm^2 in the center of a nanoparticle spot was conducted (see cutout of the

measurement in the inset of Figure 3a). The measured particle density was determined to be $\sim 2\,\mathrm{particles}/\mu\mathrm{m}^2$. The average height of the investigated gold nanoparticles was 79 nm, which corresponds well with the manufacturer's specification of 77.5 nm.

The extinction cross section $C_{ext}(\lambda)$ of a 80 nm particle was calculated using Mie-Theory (Figure 3a dashed line). Substrate effects were taken into account as in Curry et al. [29] using an effective refractive index of n_{eff} = 1.15 of the medium surrounding the particle. The calculated peak wavelength λ_{max}^{Mie} was 526.9 nm, which corresponds very well with the measured average value of μ = 529.3 nm. By employing the value of the cross section at the peak maximum $C_{ext}(\lambda_{max}^{Mie}) = 2.3 * 10^4\, nm^2$ and the averages value at the extinction maximum $Extinction(\lambda_{max}) = 0.018$ at the peak maximum we were able to estimate the particle density to be $\sim 0.8\,\mathrm{Particles}/\mu\mathrm{m}^2$. Latter value is an average over the whole spot area. The size of the AFM investigated area represents only a small fraction of the whole sensor spot area explaining the discrepancy between the determined values. However, the results are still in good agreement with the theoretical expectations.

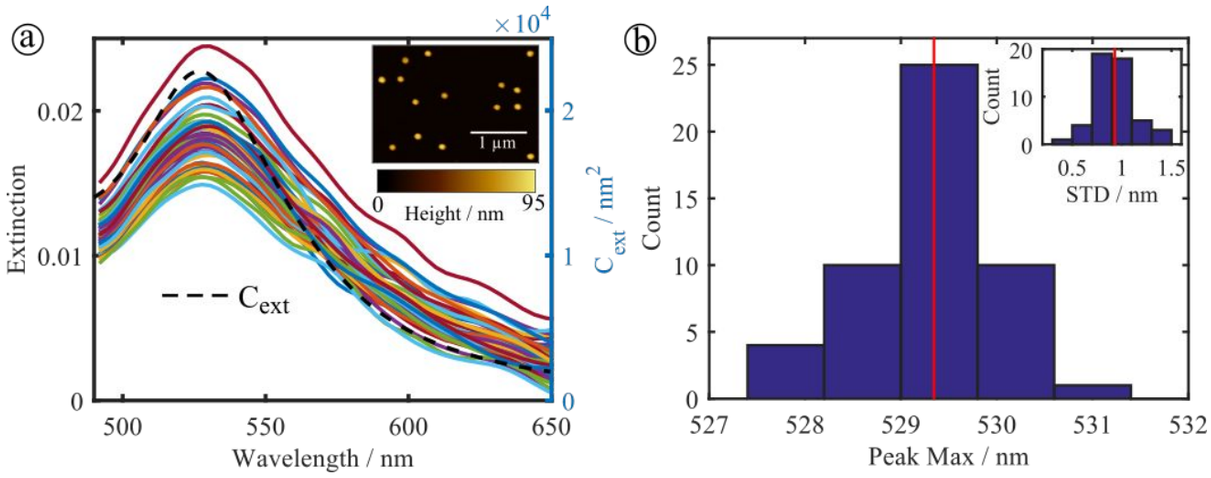

Figure 3. (a) Extinction spectra of 50 individual NP sensor spots averaged over ten measurements. The black dashed line shows the calculated extinction cross section for an 80 nm spherical gold nanoparticle. The inset shows a cutout of an AFM measurement of the center region of a sensor spot (b) Distribution of the determined peak wavelengths of the 50 individual nanoparticle spots. The vertical red line indicates the average at 529.3 nm. The inset depicts the distribution of the standard deviation (STD) of the LSPR peak maxima obtained from ten measurements.

Sensor preparation

After successful characterization of the plasmonic chip, sensor setup, and the image processing algorithm, the plasmonic chip bio-conjugation was optimized. Therefore, various capture DNA sequences (cf. Figure 7) were attached to the different sensor spots using covalent attachment on the 80 nm particles via a terminal thiol-group.

For this experiment, an ensemble of 40 nanoparticle spots was modified with five different kinds of capture DNA sequences, Cand_C, Asper_C, Pan_C, Bact1_C and Bact2_C (see Table 1) with five replicas each. Additionally, as negative control, citrate buffer (CB, representing the buffer used) was spotted on 15 nanoparticle spots (see Supporting information for spot layout). After the integration in a microfluidic flow cell, the given assay workflow was conducted.

After attachment of capture DNA, the spectroscopic response of the spots in the array was measured and plasmon peak position was determined. Figure 4a shows the distribution of LSPR positions of the extinction spectra of the nanoparticle spots after the first washing step with 5xSSC (workflow step 2, Experimental Section). Clearly visible is a separation between the negative control (citrate buffer) around 555 nm, and the DNA-modified spots with a peak higher than 556 nm. The average LSPR position of the individual DNA modified groups ranges from 556.2 nm (for the Bact2_C), to 559.1 nm for the spot modified with Bact1_C DNA sequences. The larger LSPR positions of the spots modified with DNA indicate a successful binding of the thiolated DNA on the nanoparticles at each spot. A variation of the signals in each measurement of about 2 nm is apparent. Reasons can be assumed both on the particle side (inhomogeneity of the plasmonic particle size and distribution), but also on the DNA attachment as well as on the measurement side.

Single-stranded DNA (such as the utilized capture) is known to adsorb along its strand on gold nanoparticles, lowering thereby the access for binding to complementary DNA (= hybridization), resulting in a lower efficiency of that reaction. In order to minimize this undesired adsorption, co-adsorption with a short alkanethiol like MCH is suggested [30–32]. This short molecule will – by binding of its thiol-terminus to the gold surface - cover the nanoparticle surfaces and therefore decrease the unspecific binding of DNA on the nanoparticle's surface. On the other hand, unspecific binding of the DNA somewhere else in the flow-through setup has to be minimized, which is realized by incubation with herring sperm DNA [33]. After these two steps (incubation with MCH as well with herring sperm DNA, each step followed by washing), which represents steps 3-6 of the protocol (see Experimental Section), another spectral measurement was conducted. Shifts of the peak wavelength are plotted in Figure 4b. The negative control (CB) shows no significant change, because the spectral shift induced by the MCH was below the detection limit of the hyper spectral system. However, an indirect prove of the MCH binding is given by the subsequent not binding of herring sperm DNA (This binding would induce positive LSPR shift similar to that in Figure 4a). The capture DNA show a negative shift, that means the application of MCH and then herrings sperm DNA induces a decrease in the (effective) refractive index at the particles surface. In contrast to a wider variation of measurements of the control (variation of up to 2 nm shift), the capture DNA modified particles show a narrower distribution of below 1 nm variation. The negative LSPR shift could be explained by a release of the surface-adsorbed (due to unspecific binding) DNA and conformational changes of the thiol-bound DNA strand due to the co-adsorption of MCH on the particle surface [30]. To estimate which effect dominates the induced blue shift a Mie-theory-based simulation of a core-shell nanoparticle-DNA-composition of a spherical gold nanoparticle with varying DNA confirmations was performed (see Supporting information). The

simulation shows that the after the adsorption of DNA the LSPR shift is around 2.5 nm, which is in the agreement with measured data (see figure 4a). The standing up of the DNA molecules induces a rather small blue shift (<0.5 nm) due to the decreasing sensitivity of the LSPR shift perpendicular from the surface. However, the mayor reason for the shift is desorption of not-covalently bound DNA on the surface induced by the adsorption of MCH layers, which is strong for DNA with more than 24 bases documented by Steel et al. [34]. The effect of not-covalently adsorbed DNA is especially prominent in the used single stranded DNA [35]. The simulation of standing up DNA and desorption of 50% DNA is also presented in Figure S 4 (Supporting Information) and leads to around 1.5 nm blue LSPR shift. There is no straightforward explanation of the different behavior especially of the first sequence (Cand_C) compared to the other four (like different length or the presence of certain base combinations at the end). However, as all spots are stronger blue-shifted there, it seems to be connected to the DNA sequence, which is apparently easier and/or more completely released from the surface.

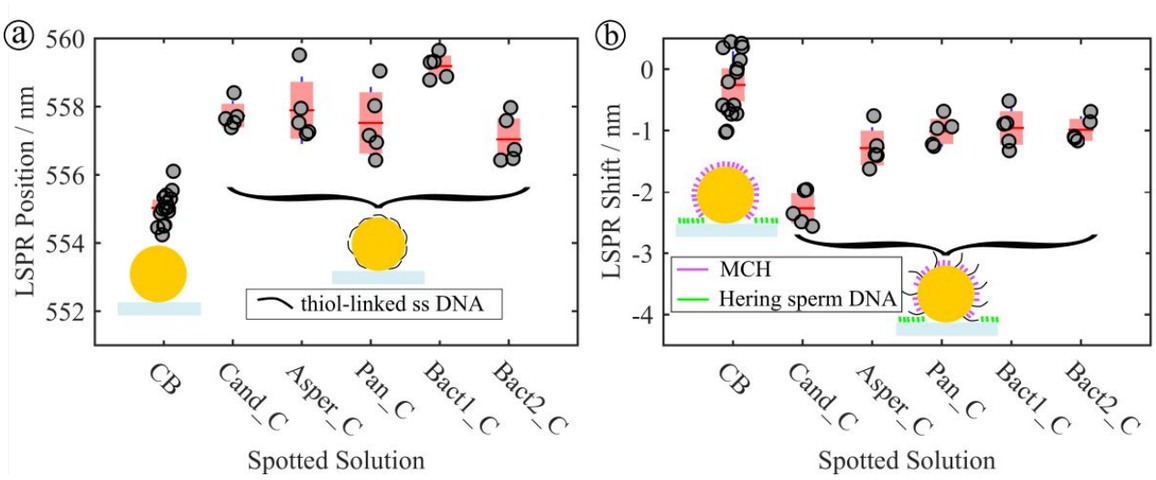

Figure 4. (a) Absolute LSPR positions of the NP spots modified (by spotting) with buffer only (negative control, CB) and various thiolated DNA solutions. (b) LSPR shift after the coadsorption with MCH and passivation with herrings sperm DNA (both by incubation the complete sample surface).

Detection of DNA target sequence

The potential of the proposed approach is demonstrated using synthetic pathogen sequences of 19-27 bases lengths as listed in table 1. Thereby, sequences from fungi involved in sepsis were utilized, including from *Candida spp.* and *Aspergillus spp.*, as well as a more general fungal sequence (Panfungal), and complemented by two bacterial pathogen sequence (Bact1 and Bact2).

In the hospital, the identification of pathogens is a key step towards an effective therapy, and can be realized using either culturing (which takes days and is therefore too long for sepsis application) or PCR. We envision a consensus PCR amplifying all fungi DNA in the patient sample, and a subsequent multiplex identification of the various individual fungi in the PCR mixture using the proposed array. Complex samples e.g. whole blood would be preprocessed by DNA purification similar as in Lehmann et al. [11] or cartridge systems to obtain pathogen DNA sequences for PCR amplification. This work-flow is simulated here using – instead of PCR products – synthetic target DNA containing the pathogen DNA sequence.

Solutions containing one target DNA sequence with a 5 nm nanoparticle label (see Figure 7) were incubated with the complete sensor array. In the case of complementary capture and target sequence, binding should be observed, which should lead to a resonance peak shift of the respective particle spot. The spectroscopic readout was conducted as described earlier.

Binding of the labeled DNA sequences was crosschecked by investigating ca. 10 mm diameter sensor areas prepared by manual pipetting as in Jatschka et al. [36]. Helium ion microscopy (HIM) [37] was conducted on such a sample after hybridization of 5 nm nanoparticle labeled DNA sequences on 80 nm spherical nanoparticles. These images confirm the efficient hybridization of the complementary DNA sequences (see Supporting Information for HIM images), which also agrees well with the spectroscopic results. Although hampered by surface charges, about five labels (5 nm particle) were visible on each larger (80 nm) nanoparticle.

Each DNA sequence was immobilized on five separated spots. The contour of these spots are in Figure 5. Each spot is false color-coded according to the averaged wavelength shift observed at this spot. Figure 5a shows the sensor response upon injection of a labeled *Aspergillus* sequence (Asper_T). On the left, the averaged extinction spectra of the individual DNA modified nanoparticle spot groups before (red) and after (blue) the injection of the labeled Asper_T-DNA sequence are shown.

The spots with a sequence complementary to *Aspergillus* (Asper_C) show the highest response with a significant signal (about 10 nm wavelength shift), some (but much less) shift is also observed for *Candida* and Bact2. This result demonstrates the high-specificity of the binding of DNA-DNA interaction in case of complementary sequences, and at the same time the quite minimal (non-measurable) unspecific binding as visible for Pan_C and Bact1_C sequence, which serve as a negative control. The low but still observable binding at Cand_C and Bact2_C can be therefore attributed to some residual base complementarity based on the utilized sequences, which could be minimized by further sequence optimization. This work is focused primarily on the demonstration of the potential of such plasmonic based bio-sensors, and therefore the evaluation of the limit-of-detection (LOD) was not carried out at this stage. However, from the presented data we can assume the limit of detection is at least 60 nM of DNA if one-to-one hybridization between the target DNA and 5nm small gold nanoparticles is achieved. Moreover, this plasmonic sensor is envisoned to be combined with DNA enrichement technique (e.g. PCR), which should allow to achieve significantly lower LOD with a yes/no answer [38].

Alternativelly, the detection scheme can be based on the observation of dehybridization of a double stranded DNA. First, the target DNA is incubated in the sensor chip. The LSPR peaks of the spots are measured, dehybridization is carried out and then the LSPR shift is measured again. The presence of the target DNA induces a negative schift at the spots with the complementary capture DNA. This approach has potential to simplify the fluid handling. In principle, DNA hybridization can be reversed using temperature increase or chemical means, in order to open the involved hydrogen bonds. A regeneration step with 10 mM HCl for 10 min was determined as the optimal chemical approach for the studied system. The HCL-based regeneration of the sensor spots is shown in Figure 5b: The removal of the previously attached target DNA with nanoparticle label results in a negative LSPR shift, which is clearly observed in the case of Asper_C sequence, and rather weakly for Cand_C. These negative LSPR shifts indicate the successful dehybridization (release of the target DNA into solution). Moreover, this dehybridization protocol can be used to regenerate the plasmonic chip in order to use the chip repeatedly.

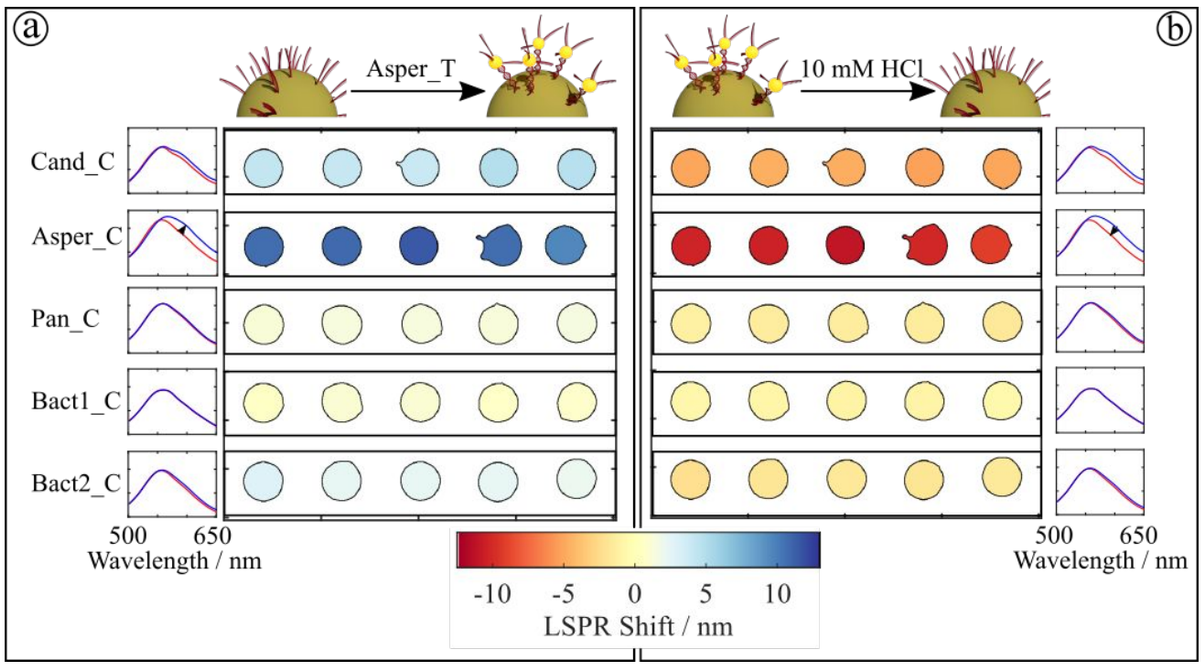

Figure 5. Sensor response of DNA modified NP spots upon the injection of Asper_T labeled DNA sequence (a) and the regeneration (dehybridization) step with HCl (b): (a) Extinction spectra averaged over all NP spots modified with a specific capture DNA sequences before (red solid line) and after (blue solid line) the injection of Asper_T labeled DNA sequence. False color image of the LSPR shifts of the DNA modified NP spots. Each spot is color coded according to its LSPR shift. (b) Extinction spectra averaged over the NP spots modified with a specific capture DNA sequences before (red solid line) and after (blue solid line) the injection of 10 mM HCl. False color image of the LSPR shifts of the DNA modified NP spots. Each spot is color coded according to its LSPR shift. The complete hybridization and the corresponding denaturation shifts of the complete assay run are depicted in the bar graphs in figure 6.

Multiplex assay

After investigating of just one target sequence (Asper_T) when incubated with the chip, now a series of different target sequences (Cand_T, Asper_T, Pan_T, Bac1_T, Bac2_T) were subsequently hybridized to the chip. After each sequence, the chip was regenerated using HCl treatment as described before. For Cand_C, Asper_C, Pan_C and the Bact1_C spots the largest LSPR shift were observed when the corresponding complementary labeled DNA sequences were injected and hybridized, with average shifts ranging from 7.2 nm to 10.7 nm indicating the specificity of the assay (Figure 6a). When Bact2_T sequence is injected the largest shifts were observed at spots modified with Asper_C capture DNA, and not – as expected – the complementary capture sequence Bact2_C. These unexpected unspecific bindings were also observed in additional measurements (see Supporting Information) and can be explained by the design of the DNA-assay. Apparently the selection of the sequences (Asper_C and Bact2) shows some homologies leading to (partial) cross complementarity. This was confirmed by in silico energy balance calculation [39] of the DNA hybridization between all capture DNA sequences and the target sequence Bact2_T (see Supporting information for further simulation details).

Note that at the denaturation step (shown in Figure 6b) after the injection of the first labeled DNA sequence (Cand_T), the negative LSPR shift upon the denaturation is smaller than the previous (positive) LSPR shift upon the hybridization event. This might be due to binding of the labeled DNA with nanoparticles on the APTES modified glass surface in close vicinity of the nanoparticles incorporated in the spot. For all subsequent hybridization and denaturation steps, the magnitude of the LSPR shifts upon hybridization and denaturation corresponds and correlates very well.

The presence of single stranded capture DNA sequences after the dehybridization on the sensor spots was verified after the chemical removal of the target sequence Bact2_T. The very same sensor array was successively re-incubated with the corresponding labeled target sequences and spectral measurements were conducted after each incubation step (workflow steps 14-16, Experimental Section). Note that the

denaturation step was omitted between the incubation steps. The measured LSPR shifts after each incubation step are shown in figure 6c. The specific and unspecific shifts are smaller compared to the first hybridization event (see figure 6a). Due to the omission of the denaturation step the corresponding capture sequences were occupied after each incubation step. Therefore, the unspecific response of the Asper_C modified spots after the incubation with the target sequences Bact2_T is not so pronounced. Two more additional measurements showing the reproducibility of the measurement are in Section Reproducibility measurement of supporting information.

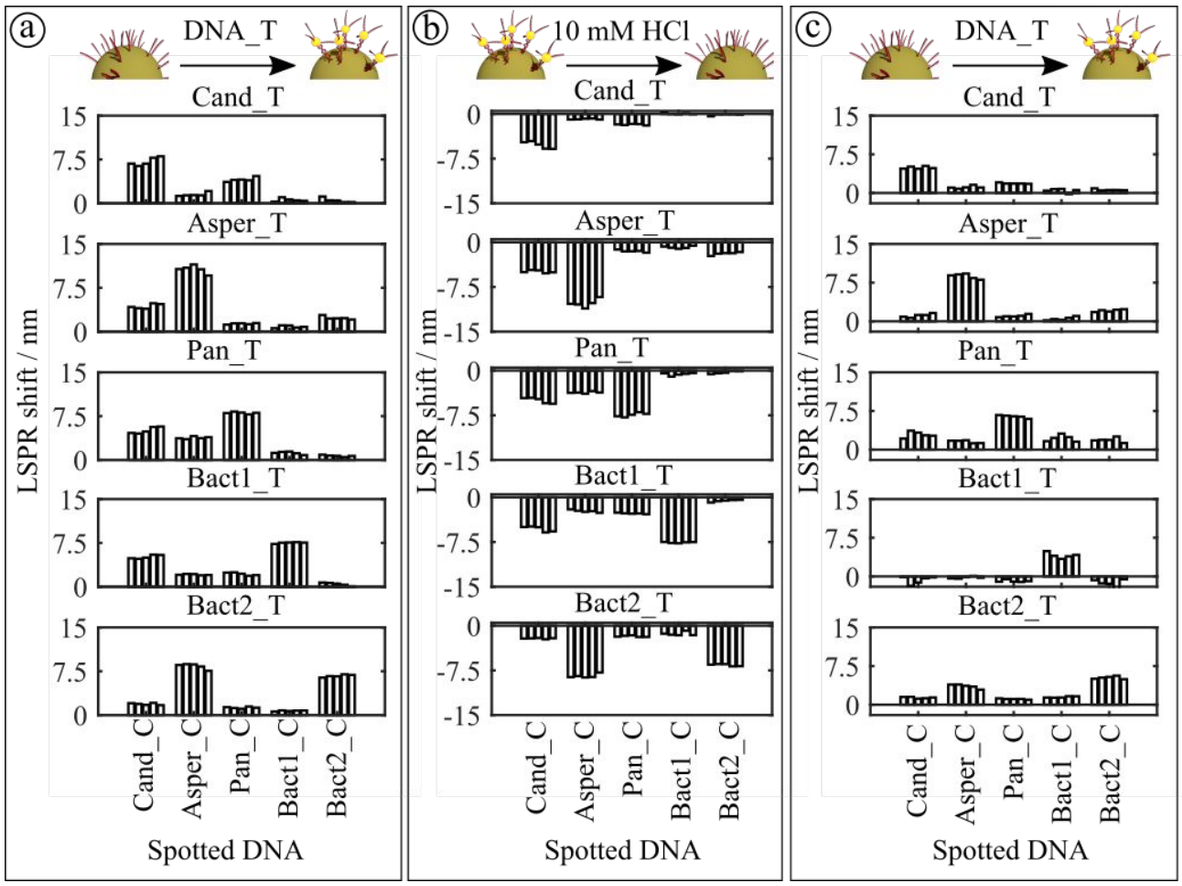

Figure 6. (a) LSPR shifts of the DNA modified sensor spots upon injection of various labeled target DNA sequences and (b) the corresponding shifts after the denaturation. After each injection of target DNA a spectral measurement was conducted, followed by a denaturation step and another measurement. (c) LSPR shifts of the DNA modified sensor spots upon the re-incubation of various labeled target DNA sequences. Note: Compared to the data shown in (a) no chemical regeneration by was conducted between the incubations with various labeled target DNA sequences.

Conclusion

The reported work demonstrates the potential of a spotted plasmonic nanoparticles array for multiplexed LSPR-based molecular detection. Various DNA sequences specific for pathogen DNA can be detected in parallel by attaching the complementary sequences as capture probes to the nanoparticle spots, and monitoring the binding using spectroscopic means. It is shown that the binding occurs highly specific depending on the sequences chosen, and that the attachment of complementary DNA can be reversed using chemical means (10 mM HCl). This regeneration allows for repeated use of the same chip for a specific detection of DNA sequences, no significant residual binding resulting in a chip aging was observed. This dehybridization can be also used as sensing principle in an assay.

Additionally the advantages of LSPR sensing in a multiplexed assay have been demonstrated. Although in the example sequences labeled by nanoparticles were used, own as well as literature results demonstrated the LSPR detection of DNA hybridization events in a label-free manner for individual measurements, which will be extended to the multiplexed approach introduced here when the utilized setup is optimized regarding its sensitivity and signal-to-noise ratio. Thereby a highly multiplexed, LSPR-based detection approach with optical readout will be realized with a variety of potential applications in biosensing and biomedical diagnostics.

Experimental Section

Materials

20 x SSC buffer, nuclease free water and, HCl were purchased from Carl Roth GmbH (Carl Roth GmbH + Co. KG, Karlsruhe, Germany). 6-Mercapto-1-hexanol, Tris(2-carboxyethyl)phosphine hydrochloride (TCEP), BSA and trisodium citrate dihydrate were purchased from Sigma (Sigma Aldrich, Munich, Germany). Citrate buffer (CB) was prepared by dissolving trisodium citrate close to a concentration of 500 mM and adjusted to pH 3.0 with concentrated HCl. Subsequently the volume was adjusted to a final concentration of 500 mM.

DNA: Capture and target sequences

All capture (DNA attached to the nanoparticle sensor) and target DNA oligonucleotides were purchased from biomers.net GmbH (Ulm, Germany) with 5'-C6-thiol modification. Before usage the thiolated DNA was treated 45 minutes with TCEP (200 x). DNA sequences from the following fungi species were used: *Aspergillus spp.* (Asper) and *Candida spp*. (Cand). As positive control a oligonucleotide (Pan_T) exhibiting a general fungal DNA sequence served as capture. As non-complementary (negative) controls, sequences (Bact1, Bact2) originating from the *Bacillus subtilis* were used where Bact2 represents an antibiotic resistance gene.

Table 1: List of capture and target DNA sequences. *Aspergillus spp.* internal transcribed spacer 2 ribosomal DNA (Asper_C/T), *Candida spp.* 16S ribosomal DNA (Cand_C/T), panfungal translation elongation factor 2 DNA (Pan_C/T), *Bacillus subtilis* PAL-related lipoprotein (slp) gene (Bact1_C/T) and β-lactase antibiotic resistance gene (Bact2_C/T).

Capture Sequences	
Name	**Sequence 5'-3'**
Asper_C	5'-Thiol C6-CAG-CAA-TGA-CGC-TCG-GAC-A- 3'
Cand_C	5'-Thiol C6-TCA-AAG-TAA-AAG-TCC-TGG-TTC-GCC-AT - 3'
Pan_C	5'-Thiol C6-AAG-GTK-TBC-CAG-GTG-AYA-AYG-TTG-GTT - 3'
Bact1_C	5'-Thiol C6-CGC-CTT-ATT-ACG-ATG-CAC-TGC-TT- 3'
Bact2_C	5'-Thiol C6-CCC-GAC-AGC-TCC-GAG-ACG-AAA-CGT- 3'
Target Sequences	
Name	**Sequence 5'-3'**
Asper_T	5'-Thiol C6-TGT-CCG-AGC-GTC-ATT-GCT-G- 3'
Cand_T	5'-Thiol C6-ATG-GCG-AAC-CAG-GAC-TTT-TAC-TTT-GA - 3'
Pan_T	5'-Thiol C6-AAC-CAA-CRT-TRT-CAC-CTG-GVA-MAC-CTT - 3'
Bact1_T	5'-Thiol C6-AAG-CAG-TGC-ATC-GTA-ATA-AGG-CG- 3'
Bact2_T	5'-Thiol C6-ACG-TTT-CGT-CTC-GGA-GCT-GTC-GGG- 3'

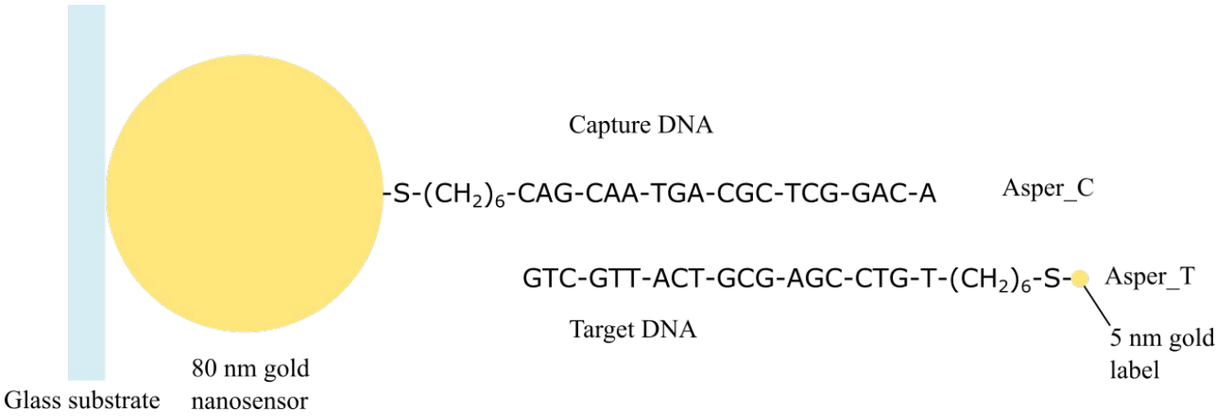

Figure 7. Schematics of the assay: A nanosensor (80 nm gold nanoparticle) on a glass substrate is functionalized with "Capture DNA" (in the example: Asper_C) which is complementary (and therefore specific binding) to a certain "Target DNA" (here: Asper_T). This Target DNA is labeled with a small (5 nm) gold nanoparticle. When the Target DNA is present in solution, it will bind to the complementary Capture DNA, and hence induces a local refractive index change, which results in a shift of the LSPR peak detected by the hyperspectral imaging system.

Labeling of the target DNA

To enhance the shift upon hybridization, 5 nm gold spherical nanoparticles were used as labels. They were prepared by a seeding growth process after Jana et al. [40], and acted as labels (see Supporting Information for extinction spectrum). The particle concentration was 31 nM [41]. The functionalization of these particles with thiolated target DNA was conducted by a modified citrate method [42]. Briefly, 1 ml of the particle solution was mixed with 20 µl of thiolated target sequences (100 µM) after TCEP treatment. This was followed by the addition of 20.81 µl citrate buffer (0.5 M; pH 3.0) and the incubation under gentle rotation (Thermomixer, Eppendorf (Germany), 400 rpm) for 30 min at room temperature. Subsequently, the solution was centrifuged (30 min at 40514 g) and 950 µl of the supernatant was removed. The pellet was re-dispensed in 200 µl water and 250 µl 10xSSC.

Substrate Preparation

Coverslips (18 mm x 18 mm x 0.17 mm, Thermo Fisher Scientific, Waltham, MA) were used for deposition of gold nanoparticles, which acted as nanosensors. The affinity of amino-functionalized surfaces for gold nanoparticles was utilized for particle immobilization. Before deposition, the substrates were cleaned successively in an ultrasonic bath with water, ethanol, acetone, Rotisol ®, ethanol and water for 10 min each. Subsequently, the slides were treated with oxygen plasma for 1 h at 380 W directly followed by silanization (Fang and Hoh 1998, modified) in 1% APTES (3-aminopropyltriethoxysilane) (Carl Roth, Karlsruhe Germany) for 10 min. After cleaning with water in an ultrasonic bath, the chips were dried under nitrogen flow and stored under argon before usage within 24 h.

Spotting and Functionalization of NP spots

Spherical gold nanoparticles with a diameter of 80 nm purchased from British BioCell International (Cardiff, UK) were 80 x concentrated by centrifugation in two steps (each 8 min at 3421 g). They were spotted by a piezoelectric dispenser system (Nanoplotter 2.1, GeSim, Grosserkmannsdorf, Germany) using a *Nano-Tip J* (GeSim, Grosserkmannsdorf, Germany), resulting in spots of about 200 µm diameter (cf. Figure. 1a). An array of nanoparticle spots (2 x 0.4 nl nanoparticle solution per spot) was generated. The center to center distance of the spots was adjusted to 400 µm. After immbolization of the nanoparticles, the chips were washed under movement in water for 10 min and dried under nitrogen flow. The substrates were treated for 1 min under ozone (UV ozone cleaner UVC-1014 NanoBioAnalytics, Berlin, Germany) before immobilization of thiolated capture DNA on the nanoparticle spots. A camera system at the print head of the piezoelectric dispenser unit allowed the

precise targeting of individual nanoparticle spots. They were then functionalized with individual DNA solution (10 x 0.4 nl 100 µM thiolated DNA capture in 250 mM CB buffer). After the immobilization the substrates were stored in the fridge at 4 °C for at least 12 h.

RGB camera imaging

RGB-images were acquired using a commercial RGB camera (AxioCam MRc 5, Zeiss, Oberkochen, Germany) attached on a microscope (AxioImager Z1.m, Zeiss, Oberkochen, Germany) in dark field illumination.

Fourier-Transform-Imaging Spectrometer

The hyperspectral imaging system is a custom-built machinery by SIOS Meßtechnik GmbH (Ilmenau, Germany) and ABS GmbH (Jena, Germany) on the basis of previous research [43].

Using the Fourier transform-based imaging spectrometer, a stack of 1402 images with varying optical path differences (OPD's) between the two arms of the interferometer is acquired in step scan mode (OPD step size = 100 nm). This image stack is normalized by subtracting an averaged dark image and division by a dark image corrected flat-field image. The flat-field image was generated by averaging over 100 images of the field of view without sample at large OPD's. The dark image is acquired likewise with turned off light source.

The normalized interferograms were processed by subtracting the dc-offset, which was determined by a linear fit, from each interferogram. The interferograms were truncated to 1024 data points in such a way that the maximum intensity is located in the center of the truncated interferograms. Apodization was performed by a cosine bell curve, blending $1/10^{th}$ of the beginnings and ends of each interferogram to zero. After these pre-processing steps a three-dimensional hyperspectral data cube $I(x,y,\lambda)$ is obtained by taking the absolute value of a pixel-wise fast Fourier transformation followed by smoothing with a Gaussian filter ($\sigma = 2$) along the third dimension. The first two dimensions of the data cube correspond to the x and y position of the field of view and the third dimension corresponds to the intensity of the image at specific wavelengths, i.e. spectral information.

Assay workflow / flow assay

The assay chip was integrated in a custom-designed microfluidic chamber (see Supporting Information) and connected to a peristaltic pump (Ismatec Reglo ICC, IDEX, Lake Forest, IL). Subsequently the flow cell was mounted on the Fourier-transform imaging spectrometer setup and the following flow/measurement assay was carried out at a flow rate of 10 µl/min. To reduce the measurement uncertainty in the determination of the plasmon peak five repetitions were conducted at each spectral measurement step and averaged:

1. 10 min washing with 5xSSC
2. **spectral measurement under continuous 5xSSC flow**
3. 15 min injection of a 10 mM 1-mercaptohexanole solution in 5x SSC (coadsorption) [31,32]
4. 10 min washing with 5xSSC
5. 15 min injection of 100 µg/ml herrings sperm DNA in 5xSSC (surface blocking)
6. 10 min washing with 5xSSC
7. **spectral measurement under continuous 5xSSC flow**
8. 20 min injection of one target DNA sequence labeled with 5 nm particles
9. 10 min washing with 5xSSC
10. **spectral measurement under continuous 5xSSC flow**
11. 10 min injection of 10 mM HCl (sensor regeneration)
12. 10 min washing with 5xSSC
13. **spectral measurement under continuous 5xSSC flow (→ 8.)**

After the 13th step the protocol repeats starting with the 8th step for other labeled DNA sequences.

Subsequently on the sensor regeneration of the last labeled target DNA, the array was incubated with various labeled target DNA sequences and hyperspectrally measured.

14. 20 min injection of one target DNA sequence labeled with 5 nm particles
15. 10 min washing with 5xSSC
16. **spectral measurement under continuous 5xSSC flow (→ 14.)**

Supporting Information

Schematic drawing and photograph image of the microfluidic chamber. Absorption spectrum and TEM image of the 5 nm gold particles. Spot layout of the assay. Helium ion microscopy images. Additional measurements on a varied spot layout. Analysis of sequence homologies of Bact2_C and Asper_T.

Acknowledgement

Funding of the research projects ImSpec (13N12836) and TRACE (02WU1348A) as well as EXASENS (13N13856) and InfectoGnostics (13GW0096F) by the Federal Ministry of Education and Research, Germany is gratefully acknowledged.

The design of the oligonucleotides used as capture was by Moldiax GmbH and Center for Sepsis Control and Care (CSCC). Lisa Stolle and the JBCI group, especially dealing with molecular biological techniques at the Leibniz-IPHT, are gratefully acknowledged for the synthesis of gold nanoparticles and provision of the microarray spotter, respectively.

References

(1) Peruski, A. H.; Peruski, L. F. Immunological Methods for Detection and Identification of Infectious Disease and Biological Warfare Agents. *Clin. Vaccine Immunol.* **2003**, *10* (4), 506–513. https://doi.org/10.1128/CDLI.10.4.506-513.2003.

(2) Foudeh, A. M.; Fatanat Didar, T.; Veres, T.; Tabrizian, M. Microfluidic Designs and Techniques Using Lab-on-a-Chip Devices for Pathogen Detection for Point-of-Care Diagnostics. *Lab Chip* **2012**, *12* (18), 3249–3266. https://doi.org/10.1039/C2LC40630F.

(3) Willner, I. Amplified Detection of Single-Base Mismatches in DNA Using Microgravimetric Quartz-Crystal-Microbalance Transduction. *Talanta* **2002**, *56* (5), 847–856. https://doi.org/10.1016/S0039-9140(01)00658-0.

(4) Patolsky, F.; Lichtenstein, A.; Willner, I. Amplified Microgravimetric Quartz-Crystal-Microbalance Assay of DNA Using Oligonucleotide-Functionalized Liposomes or Biotinylated Liposomes. *J. Am. Chem. Soc.* **2000**, *122* (2), 418–419. https://doi.org/10.1021/ja992834r.

(5) Šípová, H.; Homola, J. Surface Plasmon Resonance Sensing of Nucleic Acids: A Review. *Anal. Chim. Acta* **2013**, *773*, 9–23. https://doi.org/10.1016/j.aca.2012.12.040.

(6) Spackova, B.; Wrobel, P.; Bockova, M.; Homola, J. Optical Biosensors Based on Plasmonic Nanostructures: A Review. *Proc. IEEE* **2016**, *104* (12), 2380–2408. https://doi.org/10.1109/JPROC.2016.2624340.

(7) Palecek, E.; Fojta, M. Magnetic Beads as Versatile Tools for Electrochemical DNA and Protein Biosensing. *Talanta* **2007**, *74* (3), 276–290. https://doi.org/10.1016/j.talanta.2007.08.020.

(8) Ngom, B.; Guo, Y.; Wang, X.; Bi, D. Development and Application of Lateral Flow Test Strip Technology for Detection of Infectious Agents and Chemical Contaminants: A Review. *Anal. Bioanal. Chem.* **2010**, *397* (3), 1113–1135. https://doi.org/10.1007/s00216-010-3661-4.

(9) Craw, P.; Balachandran, W. Isothermal Nucleic Acid Amplification Technologies for Point-of-Care Diagnostics: A Critical Review. *Lab Chip* **2012**, *12* (14), 2469–2486. https://doi.org/10.1039/C2LC40100B.

(10) Craw, P.; Mackay, R.; Naveenathayalan, A.; Hudson, C.; Branavan, M.; Sadiq, S.; Balachandran, W. A Simple, Low-Cost Platform for Real-Time Isothermal Nucleic Acid Amplification. *Sensors* **2015**, *15* (9), 23418–23430. https://doi.org/10.3390/s150923418.

(11) Lehmann, L. E.; Hunfeld, K.-P.; Emrich, T.; Haberhausen, G.; Wissing, H.; Hoeft, A.; Stüber, F. A Multiplex Real-Time PCR Assay for Rapid Detection and Differentiation of 25 Bacterial and Fungal Pathogens from Whole Blood Samples. *Med. Microbiol. Immunol. (Berl.)* **2008**, *197* (3), 313–324. https://doi.org/10.1007/s00430-007-0063-0.

(12) Baker, G. C.; Ah Tow, L.; Cowan, D. A. PCR-Based Detection of Non-Indigenous Microorganisms in 'Pristine' Environments. *J. Microbiol. Methods* **2003**, *53* (2), 157–164. https://doi.org/10.1016/S0167-7012(03)00021-6.

(13) Sassolas, A.; Leca-Bouvier, B. D.; Blum, L. J. DNA Biosensors and Microarrays. *Chem. Rev.* **2008**, *108* (1), 109–139. https://doi.org/10.1021/cr0684467.

(14) Schena, M.; Shalon, D.; Davis, R. W.; Brown, P. O. Quantitative Monitoring of Gene Expression Patterns with a Complementary DNA Microarray. *Science* **1995**, *270* (5235), 467–470. https://doi.org/10.1126/science.270.5235.467.

(15) Anker, J. N.; Hall, W. P.; Lyandres, O.; Shah, N. C.; Zhao, J.; Van Duyne, R. P. Biosensing with Plasmonic Nanosensors. *Nat. Mater.* **2008**, *7* (6), 442–453.

(16) Yguerabide, J.; Yguerabide, E. E. Light-Scattering Submicroscopic Particles as Highly Fluorescent Analogs and Their Use as Tracer Labels in Clinical and Biological Applications: I. Theory. *Anal. Biochem.* **1998**, *262* (2), 137–156. https://doi.org/10.1006/abio.1998.2759.

(17) Piliarik, M.; Homola, J. Surface Plasmon Resonance (SPR) Sensors: Approaching Their Limits? *Opt. Express* **2009**, *17* (19), 16505. https://doi.org/10.1364/OE.17.016505.

(18) Yoo, S. M.; Lee, S. Y. Optical Biosensors for the Detection of Pathogenic Microorganisms. *Trends Biotechnol.* **2016**, *34* (1), 7–25. https://doi.org/10.1016/j.tibtech.2015.09.012.

(19) Haes, A. J.; Duyne, R. P. V. Preliminary Studies and Potential Applications of Localized Surface Plasmon Resonance Spectroscopy in Medical Diagnostics. *Expert Rev. Mol. Diagn.* **2004**, *4* (4), 527–537. https://doi.org/10.1586/14737159.4.4.527.

(20) Willets, K. A.; Van Duyne, R. P. Localized Surface Plasmon Resonance Spectroscopy and Sensing. *Annu. Rev. Phys. Chem.* **2007**, *58* (1), 267–297. https://doi.org/10.1146/annurev.physchem.58.032806.104607.

(21) Schneider, T.; Jahr, N.; Jatschka, J.; Csaki, A.; Stranik, O.; Fritzsche, W. Localized Surface Plasmon Resonance (LSPR) Study of DNA Hybridization at Single Nanoparticle Transducers. *J. Nanoparticle Res.* **2013**, *15* (4), 1531. https://doi.org/10.1007/s11051-013-1531-7.

(22) Ruemmele, J. A.; Hall, W. P.; Ruvuna, L. K.; Van Duyne, R. P. A Localized Surface Plasmon Resonance Imaging Instrument for Multiplexed Biosensing. *Anal. Chem.* **2013**, *85* (9), 4560–4566. https://doi.org/10.1021/ac400192f.

(23) Ahijado-Guzmán, R.; Prasad, J.; Rosman, C.; Henkel, A.; Tome, L.; Schneider, D.; Rivas, G.; Sönnichsen, C. Plasmonic Nanosensors for Simultaneous Quantification of Multiple Protein–

Protein Binding Affinities. *Nano Lett.* **2014**, *14* (10), 5528–5532. https://doi.org/10.1021/nl501865p.

(24) Rosman, C.; Prasad, J.; Neiser, A.; Henkel, A.; Edgar, J.; Sönnichsen, C. Multiplexed Plasmon Sensor for Rapid Label-Free Analyte Detection. *Nano Lett.* **2013**, *13* (7), 3243–3247. https://doi.org/10.1021/nl401354f.

(25) Xia, Y.; Whitesides, G. M. Soft Lithography. *Angew. Chem. Int. Ed.* **1998**, *37* (5), 550–575. https://doi.org/10.1002/(SICI)1521-3773(19980316)37:5<550::AID-ANIE550>3.0.CO;2-G.

(26) Lee, S.-W.; Lee, K.-S.; Ahn, J.; Lee, J.-J.; Kim, M.-G.; Shin, Y.-B. Highly Sensitive Biosensing Using Arrays of Plasmonic Au Nanodisks Realized by Nanoimprint Lithography. *ACS Nano* **2011**, *5* (2), 897–904. https://doi.org/10.1021/nn102041m.

(27) Huang, J.-S.; Callegari, V.; Geisler, P.; Brüning, C.; Kern, J.; Prangsma, J. C.; Wu, X.; Feichtner, T.; Ziegler, J.; Weinmann, P.; et al. Atomically Flat Single-Crystalline Gold Nanostructures for Plasmonic Nanocircuitry. *Nat. Commun.* **2010**, *1*, 150. https://doi.org/10.1038/ncomms1143.

(28) Dahlin, A. B.; Tegenfeldt, J. O.; Höök, F. Improving the Instrumental Resolution of Sensors Based on Localized Surface Plasmon Resonance. *Anal. Chem.* **2006**, *78* (13), 4416–4423. https://doi.org/10.1021/ac0601967.

(29) Curry, A.; Nusz, G.; Chilkoti, A.; Wax, A. Substrate Effect on Refractive Index Dependence of Plasmon Resonance for Individual Silver Nanoparticles Observed Using Darkfield Micro-Spectroscopy. *Opt. Express* **2005**, *13* (7), 2668–2677.

(30) Park, S.; Brown, K. A.; Hamad-Schifferli, K. Changes in Oligonucleotide Conformation on Nanoparticle Surfaces by Modification with Mercaptohexanol. *Nano Lett.* **2004**, *4* (10), 1925–1929. https://doi.org/10.1021/nl048920t.

(31) Herne, T. M.; Tarlov, M. J. Characterization of DNA Probes Immobilized on Gold Surfaces. *J. Am. Chem. Soc.* **1997**, *119* (38), 8916–8920. https://doi.org/10.1021/ja9719586.

(32) Levicky, R.; Herne, T. M.; Tarlov, M. J.; Satija, S. K. Using Self-Assembly To Control the Structure of DNA Monolayers on Gold: A Neutron Reflectivity Study. *J. Am. Chem. Soc.* **1998**, *120* (38), 9787–9792. https://doi.org/10.1021/ja981897r.

(33) Sambrook, J. *Molecular Cloning : A Laboratory Manual / Joseph Sambrook, David W. Russell*; Russell, D. W. (David W., 1957-, Cold Spring Harbor Laboratory, Series Eds.; Cold Spring Harbor Laboratory: Cold Spring Harbor, N.Y, 2001.

(34) Steel, A. B.; Levicky, R. L.; Herne, T. M.; Tarlov, M. J. Immobilization of Nucleic Acids at Solid Surfaces: Effect of Oligonucleotide Length on Layer Assembly. *Biophys. J.* **2000**, *79* (2), 975–981. https://doi.org/10.1016/S0006-3495(00)76351-X.

(35) Peterson, A. W. The Effect of Surface Probe Density on DNA Hybridization. *Nucleic Acids Res.* **2001**, *29* (24), 5163–5168. https://doi.org/10.1093/nar/29.24.5163.

(36) Jatschka, J.; Dathe, A.; Csáki, A.; Fritzsche, W.; Stranik, O. Propagating and Localized Surface Plasmon Resonance Sensing — A Critical Comparison Based on Measurements and Theory. *Sens. Bio-Sens. Res.* **2016**, *7*, 62–70. https://doi.org/10.1016/j.sbsr.2016.01.003.

(37) Scipioni, L.; Stern, L.; Notte, J. Applications of the Helium Ion Microscope. *Microsc. Today* **2007**, *15* (6), 12–15. https://doi.org/10.1017/S1551929500061897.

(38) Yoo, S. M.; Choi, J. Y.; Yun, J. K.; Choi, J. K.; Shin, S. Y.; Lee, K.; Kim, J. M.; Lee, S. Y. DNA Microarray-Based Identification of Bacterial and Fungal Pathogens in Bloodstream Infections. *Mol. Cell. Probes* **2010**, *24* (1), 44–52. https://doi.org/10.1016/j.mcp.2009.09.003.

(39) Zadeh, J. N.; Steenberg, C. D.; Bois, J. S.; Wolfe, B. R.; Pierce, M. B.; Khan, A. R.; Dirks, R. M.; Pierce, N. A. NUPACK: Analysis and Design of Nucleic Acid Systems. *J. Comput. Chem.* **2011**, *32* (1), 170–173. https://doi.org/10.1002/jcc.21596.

(40) Jana, N. R.; Gearheart, L.; Murphy, C. J. Seeding Growth for Size Control of 5−40 Nm Diameter Gold Nanoparticles. *Langmuir* **2001**, *17* (22), 6782–6786. https://doi.org/10.1021/la0104323.

(41) Hayat, M. A. *Colloidal Gold: Principles, Methods, and Applications*; Colloidal Gold, Three-Volume Set; Elsevier Science, 2012.

(42) Zhang, X.; Servos, M. R.; Liu, J. Instantaneous and Quantitative Functionalization of Gold Nanoparticles with Thiolated DNA Using a PH-Assisted and Surfactant-Free Route. *J. Am. Chem. Soc.* **2012**, *134* (17), 7266–7269. https://doi.org/10.1021/ja3014055.

(43) Zopf, D.; Jatschka, J.; Dathe, A.; Jahr, N.; Fritzsche, W.; Stranik, O. Hyperspectral Imaging of Plasmon Resonances in Metallic Nanoparticles. *Biosens. Bioelectron.* **2016**, *81*, 287–293. https://doi.org/10.1016/j.bios.2016.03.001.

For TOC only

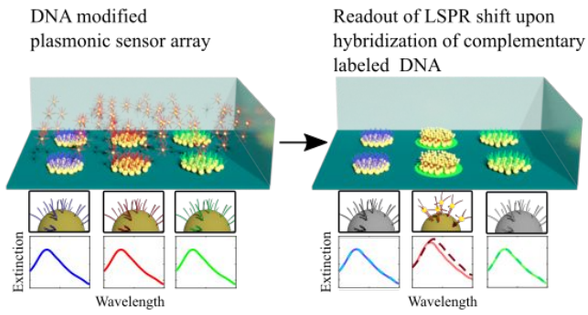
DNA modified
plasmonic sensor array
Readout of LSPR shift upon
hybridization of complementary
labeled DNA
Extinction
Wavelength
Extinction
Wavelength